Motor Current Control for High Speed Motor Drive Systems

Kantaro Yoshimoto [1)] Yuto Hirao [1)] Tomoki Yokoyama [1)]

1) Tokyo Denki University, Adachi, Tokyo, Japan

E-mail: kantaro(at)mail.dendai.ac.jp

ABSTRACT: This study examines the challenges of controlling the motor currents in low-inductance motors for high-speed motor drive systems. To achieve a compact motor design with a high-speed motor, the stator could be designed with low-inductance due to a reduced number of turns or a coreless structure. Simulation results indicate that the large current ripple causes the motor current control error in conventional vector control used for PMSMs with the current sampling technique synchronized to PWM. Through the analysis of the motor current control errors, a multi-sampling current control strategy is considered to address the motor current control errors.

KEY WORDS: high speed motor, low inductance motor, multi-sampling

1. INTRODUCTION

Traction motors used for Battery Electric Vehicles (BEVs) have been developed to minimize their size and the weight to facilitate easy installation and reduce cost[(1) (2)]. One approach to minimize moto size is to increase rotational speed and decrease torque in order to keep the output power and wheel torque with the high gear ratio of the reduction gear. For high-speed motors, high-speed homopolar-type Permanent Magnet Synchronized Motor (PMSM) designed for 100,000 min^{-1} has been proposed with low inductance value of 2 μH [(3)]. In the high-speed region, iron losses would be an issue for motor design, thus, an alternative could be coreless motors[(4)] which also have low-inductance values. With these low-inductance values, large current ripples would be caused by Pulse Width Modulation (PWM).

This study examines the challenges of controlling the motor currents in low-inductance motors for high-speed motor drive systems. Large current ripple causes motor current control errors in conventional vector control strategies used for PMSMs with the current sampling technique synchronized to PWM. Through the analysis of the motor current control errors, a multi-sampling current control strategy[(5) (6)] is proposed to address the motor current control errors.

2. CONVENTIONAL MOTOR CURRENT CONTROL

2.1. Motor current control simulation by sampling synchronized with PWM carrier using a prototype PMSM

To consider a motor current control for high speed motor, a prototype PMSM was designed to have high electrical frequency of 3300 Hz at maximum rotational speed of 8000 min^{-1}, which corresponds to the same electrical frequency as 50000 min^{-1} with 4 pole pairs. The inductance value of this prototype PMSM was 10.1 μH as the phase self-inductance in this prototype design. The purpose of this prototype motor was to evaluate the performance of the motor current control; Therefore, the rated power and the torque and the torque were designed to be small values. Before the prototyping and an experiment, the simulation was conducted on MATLAB/Simulink with Simscape electrical employing

Table 1 Simulation conditions

Max. rotational speed	8000 min^{-1}
Max. electrical frequency	3300 Hz
Number of pole pairs	24
Rated torque	1.7 Nm
d-axis inductance	10.1 μH
q-axis inductance	10.1 μH
Magnetic flux linkage	5.1 mWb
Armature resistance	10 mΩ
Inverter DC link voltage	200 V
PWM carrier frequency	40 kHz

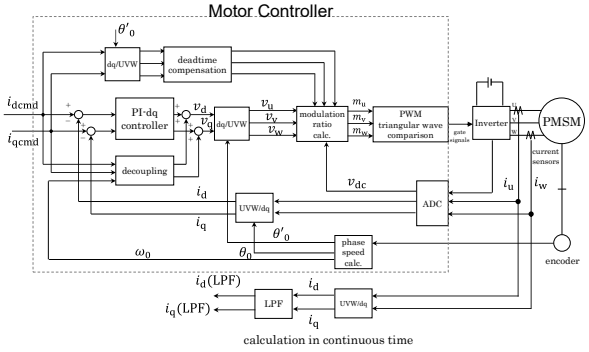

Fig. 1 block diagram of current control simulation

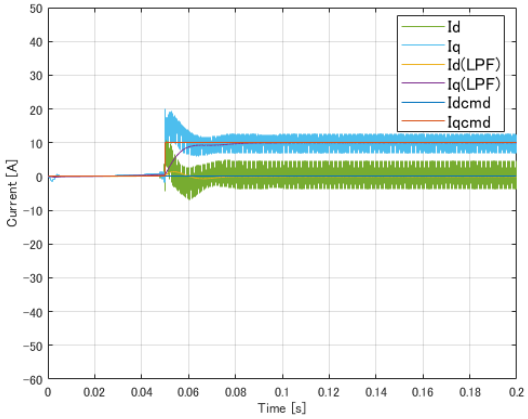

Fig. 2 dq-axes currents in controller

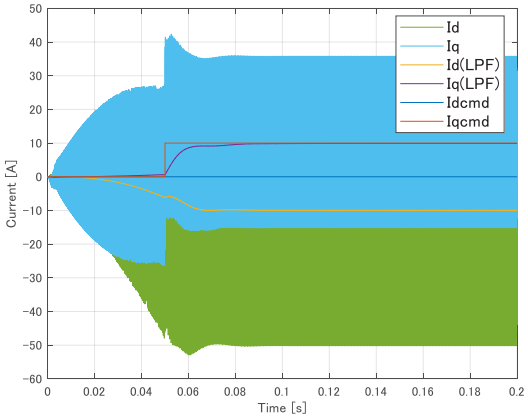

Fig. 3 dq-axes currents in continuous time

conventional motor vector control on the dq-coordinate system as shown Fig. 1. Where, PWM carrier frequency was set as 40 kHz, and DC link voltage was 200 V. Figure 2 shows the simulation results of dq-axis currents sampled in the motor controller, which the dq-axis currents were closely followed to current command well. However, the motor currents as dq-axis currents in continuous time were deviated from the current commands in Fig. 3. To identify the current control error, dq-axis currents processed through a low-pass filter (LPF) were added in Fig. 3. Especially d-axis current shows the large current offset value. It means that the sampled currents in the motor controller had the different values from the actual motor currents. The motor currents contain large sideband current ripple caused by PWM carrier. Consequently, it could be considered that the sideband current ripples as PWM carrier frequency + or – fundamental electrical frequency are converted to offset values of dq-axis currents as the fundamental electrical frequency. The dq-axis currents including these converted values of sideband current ripple were controlled to follow the dq-axis current commands. Thus, the actual motor currents were regulated as the dq-axis current commands plus the offset values caused by sideband current ripple. These current errors in low-inductance motor could lead to issues in torque control.

2.2. Analysis of motor current control error caused by synchronized with PWM carrier

To consider the cause of the current control errors in the simulation, the voltage ripple and the current ripple by PWM carrier are discussed in this subsection. The PWM carrier sideband of voltage ripple $v_{\mathrm{h}}(t)$ caused by a PWM carrier as triangular waveform with symmetrical sampling as phase voltage can be shown in (1).

$$v_{\mathrm{h}}(t) = \frac{2V_{\mathrm{dc}}}{\pi}\frac{1}{n+k\frac{\omega_0}{\omega_{\mathrm{c}}}}J_{\mathrm{k}}\left(\left(n+k\frac{\omega_0}{\omega_{\mathrm{c}}}\right)\frac{\pi}{2}M\right)\sin\left\{\left(n+k\frac{\omega_0}{\omega_{\mathrm{c}}}+k\right)\frac{\pi}{2}\right\} \times\cos\{n\omega_{\mathrm{c}}t+k\omega_0 t+n\theta_{\mathrm{c}}+k\delta\} \quad \cdots(1)$$

Where, parameters denote; V_{dc} : DC link voltage, M : modulation ratio, ω_0: fundamental electrical angular frequency, ω_{c} : PWM carrier angular frequency, k : fundamental index variable, n: PWM carrier index variable, θ_{c}: phase offset of carrier waveform , $J_{\mathrm{k}}(x)$:Bessel functions of the first kind, δ : arbitrary phase for voltage with fundamental electrical angular frequency.

The phase voltage ripple in 3-phase motor can be represented using (1) with phase $\pm 2/3\pi$. Three-phase voltage can be transformed into rotating coordinate system synchronized with the sideband frequency of PWM carrier as shown in (2)(3).

$k = 1,4,7\cdots$ or $k = -2,-5,-8\cdots$

$$\begin{bmatrix} v_{\mathrm{dh}} \\ v_{\mathrm{qh}} \end{bmatrix} = V_{\mathrm{h}}\begin{bmatrix} \cos(k\delta+n\theta_{\mathrm{c}}) \\ \sin(k\delta+n\theta_{\mathrm{c}}) \end{bmatrix} \quad \cdots(2)$$

$k = -1,-4,-7\cdots$ or $k = 2,5,8\cdots$

$$\begin{bmatrix} v_{\mathrm{dh}} \\ v_{\mathrm{qh}} \end{bmatrix} = V_{\mathrm{h}}\begin{bmatrix} \cos(k\delta+n\theta_{\mathrm{c}}) \\ -\sin(k\delta+n\theta_{\mathrm{c}}) \end{bmatrix} \quad \cdots(3)$$

The transformation matrix $\boldsymbol{C}_{\mathbf{h}}$ from 2-phase coordinate system to dhqh-coordinate system[8] is defined as (4) and (5). Equation (4) is the transformation matrix used for positive phase sequence as $k = 1,4,7\cdots$ or $k = -2,-5,-8\cdots$, and equation (5) is used for negative phase sequence as $k = -1,-4,-7\cdots$ or $k = 2,5,8\cdots$.

$$\boldsymbol{C}_{\mathbf{h}} = \begin{bmatrix} \cos\theta_{\mathrm{h}} & \sin\theta_{\mathrm{h}} \\ -\sin\theta_{\mathrm{h}} & \cos\theta_{\mathrm{h}} \end{bmatrix} = \begin{bmatrix} \cos\omega_{\mathrm{h}}t & \sin\omega_{\mathrm{h}}t \\ -\sin\omega_{\mathrm{h}}t & \cos\omega_{\mathrm{h}}t \end{bmatrix} \quad \cdots(4)$$

$$\boldsymbol{C}_{\mathbf{h}} = \begin{bmatrix} \cos\theta_{\mathrm{h}} & -\sin\theta_{\mathrm{h}} \\ \sin\theta_{\mathrm{h}} & \cos\theta_{\mathrm{h}} \end{bmatrix} = \begin{bmatrix} \cos\omega_{\mathrm{h}}t & -\sin\omega_{\mathrm{h}}t \\ \sin\omega_{\mathrm{h}}t & \cos\omega_{\mathrm{h}}t \end{bmatrix} \quad \cdots(5)$$

Here, the harmonic electrical angle θ_{h} is shown using the harmonic electrical angular frequency $\omega_{\mathrm{h}} = \pm k\omega_0 + n\omega_{\mathrm{c}}$.

On dhqh-coordinate system synchronized with the sideband frequency of PWM carrier, the voltage amplitude of $v_{\mathrm{h}}(t)$ is

expressed as V_{h}, and voltage of dhqh-axis are defined as v_{dh} and v_{qh}. The circuit equation on dhqh-axis is led as (6)(7), therefore, dhqh-currents $i_{\mathrm{dh}}, i_{\mathrm{qh}}$ as steady state can be represented in (8)(9).

$k = 1,4,7\cdots$ or $k = -2,-5,-8\cdots$

$$\begin{bmatrix} v_{\mathrm{dh}} \\ v_{\mathrm{qh}} \end{bmatrix} = \begin{bmatrix} R & -\dfrac{L_{\mathrm{d}}+L_{\mathrm{q}}}{2}\omega_{\mathrm{h}} \\ \dfrac{L_{\mathrm{d}}+L_{\mathrm{q}}}{2}\omega_{\mathrm{h}} & R \end{bmatrix} \begin{bmatrix} i_{\mathrm{dh}} \\ i_{\mathrm{qh}} \end{bmatrix} + \frac{L_{\mathrm{d}}+L_{\mathrm{q}}}{2}\frac{d}{dt}\begin{bmatrix} i_{\mathrm{dh}} \\ i_{\mathrm{qh}} \end{bmatrix} \quad \cdots (6)$$

$k = -1,-4,-7\cdots$ or $k = 2,5,8\cdots$

$$\begin{bmatrix} v_{\mathrm{dh}} \\ v_{\mathrm{qh}} \end{bmatrix} = \begin{bmatrix} R & \dfrac{L_{\mathrm{d}}+L_{\mathrm{q}}}{2}\omega_{\mathrm{h}} \\ -\dfrac{L_{\mathrm{d}}+L_{\mathrm{q}}}{2}\omega_{\mathrm{h}} & R \end{bmatrix} \begin{bmatrix} i_{\mathrm{dh}} \\ i_{\mathrm{qh}} \end{bmatrix} + \frac{L_{\mathrm{d}}+L_{\mathrm{q}}}{2}\frac{d}{dt}\begin{bmatrix} i_{\mathrm{dh}} \\ i_{\mathrm{qh}} \end{bmatrix} \quad \cdots (7)$$

$k = 1,4,7\cdots$ or $k = -2,-5,-8\cdots$

$$\begin{bmatrix} i_{\mathrm{dh}} \\ i_{\mathrm{qh}} \end{bmatrix} = \frac{2V_{\mathrm{h}}}{(L_{\mathrm{d}}+L_{\mathrm{q}})\omega_{\mathrm{h}}}\begin{bmatrix} \sin(k\delta+n\theta_{\mathrm{c}}) \\ -\cos(k\delta+n\theta_{\mathrm{c}}) \end{bmatrix} \quad \cdots (8)$$

$k = -1,-4,-7\cdots$ or $k = 2,5,8\cdots$

$$\begin{bmatrix} i_{\mathrm{dh}} \\ i_{\mathrm{qh}} \end{bmatrix} = \frac{2V_{\mathrm{h}}}{(L_{\mathrm{d}}+L_{\mathrm{q}})\omega_{\mathrm{h}}}\begin{bmatrix} \sin(k\delta+n\theta_{\mathrm{c}}) \\ \cos(k\delta+n\theta_{\mathrm{c}}) \end{bmatrix} \quad \cdots (9)$$

Equations (8) and (9) are transformed into dq-coordinate system from dhqh-coordinate system to consider the dq-axis current errors caused. The inverse transformation matrix $\boldsymbol{C_{\mathrm{h}}^{-1}}$ and transformation matrix $\boldsymbol{C}$ are used for this transformation as (10) in case of positive phase sequence. As similar way, the transformation for negative phase sequence is shown in (11).

$k = 1,4,7\cdots$ or $k = -2,-5,-8\cdots$

$$\begin{aligned} \boldsymbol{C}\boldsymbol{C_{\mathrm{h}}^{-1}} &= \begin{bmatrix} \cos\omega_0 t & \sin\omega_0 t \\ -\sin\omega_0 t & \cos\omega_0 t \end{bmatrix}\begin{bmatrix} \cos\omega_{\mathrm{h}} t & -\sin\omega_{\mathrm{h}} t \\ \sin\omega_{\mathrm{h}} t & \cos\omega_{\mathrm{h}} t \end{bmatrix} \\ &= \begin{bmatrix} \cos(\omega_0-\omega_{\mathrm{h}})\,t & \sin(\omega_0-\omega_{\mathrm{h}})t \\ -\sin(\omega_0-\omega_{\mathrm{h}})t & \cos(\omega_0-\omega_{\mathrm{h}})\,t \end{bmatrix} \quad \cdots (10) \end{aligned}$$

$k = -1,-4,-7\cdots$ or $k = 2,5,8\cdots$

$$\begin{aligned} \boldsymbol{C}\boldsymbol{C_{\mathrm{h}}^{-1}} &= \begin{bmatrix} \cos\omega_0 t & \sin\omega_0 t \\ -\sin\omega_0 t & \cos\omega_0 t \end{bmatrix}\begin{bmatrix} \cos\omega_{\mathrm{h}} t & \sin\omega_{\mathrm{h}} t \\ -\sin\omega_{\mathrm{h}} t & \cos\omega_{\mathrm{h}} t \end{bmatrix} \\ &= \begin{bmatrix} \cos(\omega_0+\omega_{\mathrm{h}})\,t & \sin(\omega_0+\omega_{\mathrm{h}})t \\ -\sin(\omega_0+\omega_{\mathrm{h}})t & \cos(\omega_0+\omega_{\mathrm{h}})\,t \end{bmatrix} \quad \cdots (11) \end{aligned}$$

In case of $k = 1, n = 2, \theta_{\mathrm{c}} = \pi$, dq-axis currents $i_{\mathrm{d12}}, i_{\mathrm{q12}}$ in (12) can be led from (8).

$$\begin{bmatrix} i_{\mathrm{d12}} \\ i_{\mathrm{q12}} \end{bmatrix} = \frac{2V_{\mathrm{h}}}{(L_{\mathrm{d}}+L_{\mathrm{q}})\omega_{\mathrm{h}}}\begin{bmatrix} \cos 2\omega_c t & -\sin 2\omega_c t \\ \sin 2\omega_c t & \cos 2\omega_c t \end{bmatrix}\begin{bmatrix} \sin\delta \\ -\cos\delta \end{bmatrix} \cdots (12)$$

When phase currents of PMSM are sampled at each beginning of PWM carrier, time t in (12) can be replaced with product of T_s : sampling period equal to PWM carrier period and N: number of sampling.

$$\begin{aligned} \begin{bmatrix} i_{\mathrm{d12}} \\ i_{\mathrm{q12}} \end{bmatrix} &= \frac{2V_{\mathrm{h}}}{(L_{\mathrm{d}}+L_{\mathrm{q}})\omega_{\mathrm{h}}}\begin{bmatrix} \cos 4\pi N & -\sin 4\pi N \\ \sin 4\pi N & \cos 4\pi N \end{bmatrix}\begin{bmatrix} \sin\delta \\ -\cos\delta \end{bmatrix} \\ &= \frac{2V_{\mathrm{h}}}{(L_{\mathrm{d}}+L_{\mathrm{q}})\omega_{\mathrm{h}}}\begin{bmatrix} \sin\delta \\ -\cos\delta \end{bmatrix} \quad \cdots (13) \end{aligned}$$

Equation (13) shows that the harmonic currents with $k = 1$ take the offset values on dq-axis by sampling synchronized with PWM carrier. In the same way, in case of $k = -1$, the harmonic currents take the offset values on dq-axis. In case of $k \neq \pm 1$, equations (10)(11) show that the PWM carrier sideband currents can not be transformed into the offset value on dq-coordinate system. From this analysis, it can be considered that the sum of the offset currents as sideband $k = \pm 1$ of PWM carrier causes the current control errors.

3. MULTI SAMPLING MOTOR CURRENT CONTROL

3.1. Multi-sampling method to avoid the offset error

From the consideration of offset currents on dq-axis currents caused by PWM carrier sideband of voltage ripple, the several approaches can solve this issue. First, increasing ω_{h} with higher ω_{c} in (10) or (11) can reduce the values of $i_{\mathrm{d12}}, i_{\mathrm{q12}}$. However, high ω_{c} increases the switching loses of the inverter. One of other ideas is to sample the phase currents with higher sampling frequency in order that $\cos 2\omega_{\mathrm{c}} t$ and $\sin 2\omega_{\mathrm{c}} t$ in (12) do not take constat values. Using sampling period T_{s} and PWM carrier period T_{c}, equation (14) can be represented from (12).

$$\begin{bmatrix} i_{\mathrm{d12}} \\ i_{\mathrm{q12}} \end{bmatrix} = \frac{2V_{\mathrm{h}}}{(L_{\mathrm{d}}+L_{\mathrm{q}})\omega_{\mathrm{h}}}\begin{bmatrix} \cos 4\pi N\frac{T_s}{T_c} & -\sin 4\pi N\frac{T_s}{T_c} \\ \sin 4\pi N\frac{T_s}{T_c} & \cos 4\pi N\frac{T_s}{T_c} \end{bmatrix}\begin{bmatrix} \sin\delta \\ -\cos\delta \end{bmatrix} \quad \cdots (14)$$

From (14), the sampling period T_{s} must be designed smaller than $T_{\mathrm{c}}/2$. If other harmonic components of $k = \pm 1$ would have large values, the sampling period T_{s} can be considered using T_{c}/n.

3.1. Motor current control by multi-sampling method

For the current errors in low inductance motor, the multi-sampling method can be useful. Multi-sampling control methods using Field Programmable Gate Array (FPGA) [5] [6] have been proposed and show good robustness and high response performance. The strategy of the multi-sampling method current control using FPGA is shown in Fig.4, which can be explained in 4 modes. During mode 1 and mode 3, the current value can be sampled through high-speed A/D converter, then the dq-conversion and the current feedback control are calculated in fast

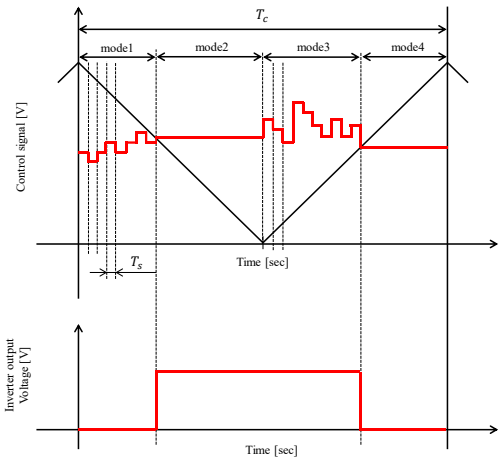

Fig. 4 Multi-sampling current control and its PWM comparison strategy

control period as MHz order. The output signal as modulation ratio can be updated at sampling and control period T_s . Once carrier comparison happened, the modulation ration should not be updated to avoid additional switching in mode 2 and mode 4. By implementing mode 2 and mode 4, PWM switching frequency can be kept as same as the original PWM carrier frequency, otherwise, the multi-sampling control would cause a greater number of switching.

Figure 5 shows the simulation results of controlled by the multi-sampling control. Here, the multi-sampling controller had PI dq-axis current controller and sampling period was set to 10 MHz. Id (LPF) and Iq (LPF) show the dq-axis current in continuous time with LPF to evaluate the offset current caused by PWM. From the simulation results, Id (LPF) and Iq (LPF) were controlled to follow the command without offset value compared with Fig.3.

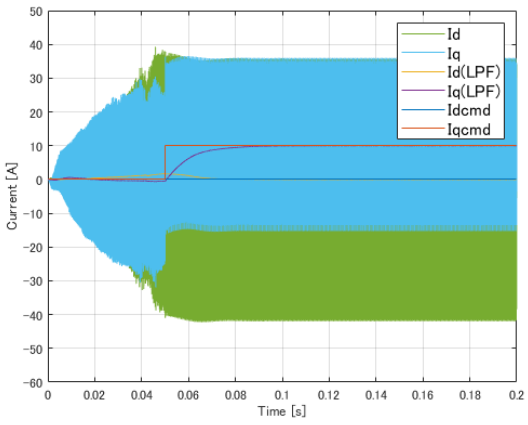

Fig. 5 dq-axes currents in continuous time by multi-sampling current control

4. CONCLUSIONS

This study discussed the issues as the motor current control error in the low inductance motors. Then, the multi-sampling current control strategy was applied to solve the current control error and it was validated through the motor control simulation. Towards final manuscripts, the prototype motor with electrical frequency of 3300 Hz will be tested to verify the issues and the effectiveness of the multi-sampling controller.

ACKNOWLEDGMENT

This study is based on results obtained from a subcontract from Transmission Research Association for Mobility Innovation (TRAMI) as part of the New Energy and Industrial Technology Development Organization (NEDO) Feasibility Study Program on Energy and New Environmental Technology / Resource saving of electric drive system for automobiles by ultra-high rotation of e-motor. (JPNP14004).

REFERENCES

(1) S. Oki, Y. Sato, “Nissan LEAF and e-POWER: Evolution of Motors and Inverters,” *IEEJ Journal of Industry Applications*, Vol.13, No.1, pp. 8-16, 2024.
(2) K. Yoshimoto, T. Hanyu, “ NISSAN e-POWER: 100% Electric Drive and Its Powertrain Control,” *IEEJ Journal of Industry Applications*, Vol.10, No.4, pp. 411-416, 2021.
(3) T. Kosaka, C. Higashihama, T. Ishihara, H. Matsumori and N. Matsui, "Design Study on Light-weight Quasi-coreless SPMSM using CFRP, Small Amount of SMC Core and Aluminum Winding," *2023 11th International Conference on Power Electronics and ECCE Asia (ICPE 2023 - ECCE Asia)*, pp. 2338-2343, 2023.
(4) H. Arita, K. Nishiwaki, M. Iezawa and T. Kosaka, “High Speed Homopolar Type Permanent Magnet Motor Designed for Fast Acceleration Response,” *IEEJ Journal of Industry Applications*, Vol. 11, No. 6, pp. 763-770, 2022.
(5) D. Hiroe, X. Zhang, K.Nakamura, K.Sato, R.Suzuki, K.Yoshimoto, T.Yokoyama, “A Study of 10MHz Multi-Sampling Deadbeat Control for PMSM Drive System using USPM Controller,” *IEEJ Journal of Industry Applications*, Vol.12, No.3, pp. 508-516, 2023.
(6) D. Hiroe, X. Zhang, K. Yoshimoto and T. Yokoyama, "Parameter Estimation Method of Ultra Robust 10MHz Multi-sampling Disturbance Compensation Deadbeat Control for PMSM Drive Using USPM Controller," *2023 IEEE Energy Conversion Congress and Exposition (ECCE)*, pp. 4236-4242, 2023.
(7) D. Grahame Holmes, Thomas A. Lipo, “Pulse Width Modulation for Power Converters: Principles and Practice,” A JOHN WILEY & SONS, INC., PUBLICATION, 2003
(8) K. Yoshimoto, Y. Kitajima, “A Novel Harmonic Current Control for IPMSMs,” *International Power Electronics Conference* (*IPEC-Niigata 2005*), 2005.